THE JOURNAL OF BIOLOGICAL CHEMISTRY VOL. 285, NO. 6, pp. 4060–4073, February 5, 2010

Tumor Necrosis Factor-α Regulates Transforming Growth Factor-β-dependent Epithelial-Mesenchymal Transition by Promoting Hyaluronan-CD44-Moesin Interaction*[S]

Received for publication, August 18, 2009, and in revised form, December 3, 2009 Published, JBC Papers in Press, December 4, 2009, DOI 10.1074/jbc.M109.056523

Eri Takahashi[‡§], Osamu Nagano[‡¶], Takatsugu Ishimoto[‡], Toshifumi Yae[‡], Yoshimi Suzuki[‖], Takeshi Shinoda[‖], Satoshi Nakamura[‖], Shinichiro Niwa[‖], Shun Ikeda[**], Hisashi Koga[**], Hidenobu Tanihara[§], and Hideyuki Saya[‡¶1]

From the [‡]Division of Gene Regulation, Institute for Advanced Medical Research, School of Medicine, Keio University, Tokyo 160-8582, the [§]Department of Ophthalmology and Visual Science, Graduate School of Medical Sciences, Kumamoto University, Kumamoto 860-8556, the [¶]Japan Science and Technology Agency, CREST, Tokyo 102-0075, the [‖]Department of Biomedical Research and Development, Link Genomics Inc., Tokyo 103-0024, and the [**]Laboratory of Medical Genomics, Department of Human Genome Research, Kazusa DNA Research Institute, Chiba 292-0818, Japan

Aberrant epithelial-mesenchymal transition (EMT) is involved in development of fibrotic disorders and cancer invasion. Alterations of cell-extracellular matrix interaction also contribute to those pathological conditions. However, the functional interplay between EMT and cell-extracellular matrix interactions remains poorly understood. We now show that the inflammatory mediator tumor necrosis factor-α (TNF-α) induces the formation of fibrotic foci by cultured retinal pigment epithelial cells through activation of transforming growth factor-β (TGF-β) signaling in a manner dependent on hyaluronan-CD44-moesin interaction. TNF-α promoted CD44 expression and moesin phosphorylation by protein kinase C, leading to the pericellular interaction of hyaluronan and CD44. Formation of the hyaluronan-CD44-moesin complex resulted in both cell-cell dissociation and increased cellular motility through actin remodeling. Furthermore, this complex was found to be associated with TGF-β receptor II and clathrin at actin microdomains, leading to activation of TGF-β signaling. We established an *in vivo* model of TNF-α-induced fibrosis in the mouse eye, and such ocular fibrosis was attenuated in CD44-null mice. The production of hyaluronan and its interaction with CD44, thus, play an essential role in TNF-α-induced EMT and are potential therapeutic targets in fibrotic disorders.

The epithelial-mesenchymal transition (EMT)[2] of epithelial cells is characterized by the loss of epithelial characteristics and the gain of mesenchymal attributes. During this transition, epithelial cells down-regulate cell-cell adhesion systems, lose their polarity, and acquire a mesenchymal phenotype associated with increased interaction with the extracellular matrix (ECM) and enhanced migratory capacity. The EMT is considered a critical event in metazoan embryogenesis as well as in physiological processes such as wound healing. However, it also plays an important role in pathological settings such as fibrotic disorders in various organs as well as cancer invasion and metastasis.

The EMT associated with physiological processes is triggered by members of the transforming growth factor-β (TGF-β) family of proteins that function as morphogens (1). *In vitro* studies have also shown that TGF-β is the major inducer of the EMT in epithelial cells (2). Fibrotic disorders associated with pathological EMT result from a series of events including inflammation, leukocyte infiltration, and the production of cytokines and growth factors. TGF-β is one of the cytokines produced during inflammation and is, therefore, thought to heavily contribute to EMT-associated fibrosis (3). However, given that TGF-β also possesses anti-inflammatory properties, the mechanism of pathological EMT induced by the inflammatory response may be multifactorial and differ from that of physiological EMT.

In addition to growth factors, changes in the ECM microenvironment contribute to the EMT. Epithelial cells cultured in a type I collagen gel were found to undergo the EMT (4). Furthermore, collagen-induced changes in cadherin expression and cell morphology in epithelial cells were shown to be dependent on activation of intracellular signaling by collagen (5). These observations implicated signaling pathways activated by cell adhesion to the ECM in acquisition of the mesenchymal phenotype. Hyaluronic acid (HA), or hyaluronan, is a major component of the ECM and plays a key role in tissue homeostasis as well as in pathological tissue remodeling (6). HA is synthesized by hyaluronic acid synthases (HASs) located at the plasma membrane. Three isoforms of mammalian HAS catalyze the

* This work was supported in part by grants from the Ministry of Education, Culture, Sports, Science, and Technology of Japan (to O. N. and H. S.) and by a grant from the National Institute of Biomedical Innovation, Japan (to H. S.).

[S] The on-line version of this article (available at http://www.jbc.org) contains supplemental Table 1 and Movies 1–5.

The raw data described in this study have been deposited in the Gene Expression Omnibus data base (www.ncbi.nlm.nih.gov) under the accession number GSE12548.

[1] To whom correspondence should be addressed: Division of Gene Regulation, Institute for Advanced Medical Research, School of Medicine, Keio University, 35 Shinano-machi, Shinjuku-ku, Tokyo 160-8582, Japan. Tel.: 81-3-5363-3981; Fax: 81-3-5363-3982; E-mail: hsaya@a5.keio.jp.

[2] The abbreviations used are: EMT, epithelial-mesenchymal transition; ECM, extracellular matrix; TNF, tumor necrosis factor; TGF, transforming growth factor; HA, hyaluronic acid; HAS, hyaluronic acid synthase; ERM, ezrin-radixin-moesin; pERM, phosphorylated ERM; RPE cells, retinal pigment epithelial cells; α-SMA, α-smooth muscle actin; EAFD, EMT-associated fibrotic deposit; 4-MU, 4-methylumbelliferone; PKC, protein kinase C; MAPK, mitogen-activated protein kinase; siRNA, small interfering RNA; RT, reverse transcription; PVR, proliferative vitreoretinopathy; PBS, phosphate-buffered saline; DIC, differential interference contrast.

synthesis of HA of distinct molecular sizes. HAS1 and HAS2 synthesize high molecular mass HA (200–2000 kDa), whereas HAS3 synthesizes low molecular mass HA (100–1000 kDa) (7). HAS2-deficient mice fail to manifest the characteristic transformation of cardiac endothelial cells into mesenchyme (8). In addition, oligosaccharide forms of HA, which inhibit binding of endogenous HA to the HA receptor CD44, attenuate the EMT associated with cardiac development (9–11). These findings implicate HA-dependent changes in the tissue microenvironment in induction of the EMT.

CD44 is the principal transmembrane adhesion receptor for HA and plays a central role in the remodeling and degradation of HA that lead to cell migration as well as to cancer invasion and metastasis (12, 13) The cytoplasmic tail of CD44 recruits ezrin-radixin-moesin (ERM) proteins that are linked to the actin cytoskeleton and thereby promote cell motility. Expression of CD44 is up-regulated not only in cancer cells but also in cells associated with inflammatory diseases (14–16), and inflammation-mediated fibrosis in the lung and kidney was shown to be attenuated in CD44-deficient mice (17–20). However, the molecular mechanism by which the HA-CD44 interaction leads to the development of fibrotic disorders remains largely unknown.

Proliferative vitreoretinopathy (PVR) is a disorder characterized by the formation of membranes on the surfaces of the retina and within the vitreous cavity after retinal detachment surgery, and intraocular inflammation and EMT are thought to be the pathogenesis of this disease (21, 22). The PVR membrane consists of extracellular matrix, retinal pigment epithelium (RPE), retinal glial cells, fibroblasts, and inflammatory macrophages (23, 24). Intravitreal cell injection models of PVR show that not only fibroblasts, but also RPE cells, are associated with the formation of intraocular membrane (25). Various growth factors and cytokines, which are inflammatory products of cell activation, were increased in vitreous aspirates from the eyes with PVR. One of the most prominent of the inflammatory cytokines is tumor necrosis factor-α (TNF-α), whose mRNA and proteins are widely expressed in PVR membranes (21, 26) TNF-α is mainly derived from activated macrophages, and RPE and glial cells in PVR membranes also releases it (27). Although TNF-α is thought to play a causative role in PVR, the underlying mechanism is unknown.

We have now developed an *in vitro* model of EMT-associated fibrosis based on human RPE cells. With the use of this model, we identified TNF-α as an important inducer of EMT-associated fibrotic focus formation. In addition, we clarified that the HA-CD44-moesin interaction triggered by TNF-α is required for activation of TGF-β signaling that leads to induction of the mesenchymal phenotype in RPE cells. Furthermore, fibrosis induced by injection of TNF-α into the mouse retina was found to be markedly suppressed in CD44 knock-out mice. These findings indicate that the HA-CD44 interaction plays a key role in EMT-associated fibrotic disorders.

EXPERIMENTAL PROCEDURES

Cell Culture—ARPE-19 cells were obtained from American Type Culture Collection and maintained in Dulbecco's modified Eagle's medium-nutrient mixture F-12 (Sigma) supplemented with 10% fetal bovine serum. All experiments were performed in serum-free medium unless otherwise noted.

Reagents and Antibodies—Human recombinant TNF-α and the active form of human recombinant TGF-β2 were obtained from R&D Systems; 4-methylumbelliferone (4-MU) was from Wako, GF109203X, Y-27632, and SB203580 were from Calbiochem, SB431542 was from Nacalai Tesque, and hyaluronidase *Streptococcus dysgalactiae* was from Seikagaku. Antibodies used in the study were as follows: the anti-phosphorylated form of ERM and anti-phospho-Smad2 (Calbiochem); anti-ERM (Chemicon); anti-clathrin heavy chain and anti-caveolin1 (BD Transduction Laboratories); anti-Smad2 (Cell Signaling); anti-CD44 (BU52) for immunoblot analysis and immunofluorescence staining (Ancell); anti-CD44 (IM-7.8.1) for blocking HA-CD44 binding (BioLegend); anti-N-cadherin (Calbiochem and Santa Cruz Biotechnology); anti-moesin for immunofluorescence staining, anti-ezrin, and anti-cytokeratin 18 as well as anti-CD44 (F10-44-2) for immunoprecipitation (Abcam); anti-TGF-β receptor II (Cell Signaling and Santa Cruz Biotechnology), anti-smooth muscle actin (α-SMA) and anti-α-tubulin (Sigma); anti-fibronectin (NeoMarkers); anti-moesin for immunoblot analysis (kindly provided by S. Tsukita, Osaka University).

Plasmids and Small Interfering RNA (siRNA) Transfection—The sequences of siRNA (chimeric RNA-DNA) duplexes (Japan Bioservice) were 5′-AAAUGGUCGCUACAGCAUCTT-3′ and 5′-GAUGCUGUAGCGACCAUUUTT-3′ for human CD44 (28), 5′-CUAUACAUGCGCCGUCGCATT-3′ and 5′-UGCGACGGCGCAUGUAUAGTT-3′ for human moesin, and 5′-CGUACGCGGAAUACUUCGATT-3′ and 5′-UCGAAGUAUUCCGCGUACGTT-3′ for luciferase (GL-2) as a control. Cells were transfected with the annealed siRNAs for 48 h with the use of the Oligofectamine reagent (Invitrogen).

Immunoprecipitation and Immunoblot Analysis—Immunoprecipitation followed by immunoblot analysis was performed as previously described (29). In brief, cells were lysed on ice for 20 min, and the lysates were incubated for 2 h with antibodies to CD44 or TGF-β receptor II, after which protein A-Sepharose beads (GE Healthcare) were added, and the mixture was incubated for an additional 2 h. The beads were isolated by centrifugation, and the bead-bound proteins were subjected to immunoblot analysis.

Immunofluorescence Microscopy—Immunofluorescence microscopic analysis was performed as previously described (30). In brief, ARPE-19 cells were fixed with 4% paraformaldehyde and incubated for 60 min with primary antibodies or biotinylated HA-binding protein (Seikagaku). The cells were then washed 3 times with phosphate-buffered saline (PBS) before incubation for 60 min with secondary antibodies labeled with either fluorescein isothiocyanate (BIOSOURCE) or Texas Red (Invitrogen). Biotinylated HA-binding protein was detected by fluorescein isothiocyanate-conjugated avidin (Invitrogen). Actin fibers were visualized by staining with Alexa Fluor 488-labeled phalloidin (Invitrogen). The cells were mounted in 80% glycerol or Vectashield mounting medium with propidium iodide (Vector) and visualized with a confocal microscope (Fluoview, Olympus).

Microarray and Reverse Transcription (RT)-PCR Analyses—Total RNA was extracted from cells with the use of Trizol reagent (Invitrogen). For microarray analysis, biotin-labeled cRNA probes synthesized from the total RNA were subjected to hybridization with a GeneChip Human Genome U133 Plus 2.0 Array (Affymetrix), and hybridization was visualized with streptavidin-phycoerythrin. Raw intensity data for each experiment were first normalized by the MAS5.0 statistical algorithm (Affymetrix) and then $\log_2$-transformed for calculation of Z scores. The scores were calculated by subtracting the overall average gene intensity (within a single experiment) from the raw intensity data for each gene and then dividing the result by the standard deviation of all the measured intensities according to a previously established formula (31). Further statistical analysis was performed by analysis of variance (32).

For RT-PCR analysis, portions (2 μg) of total RNA were subjected to RT with an oligo(dT) primer and Superscript II reverse transcriptase (Invitrogen). PCR was performed as previously described (33) with the primers (forward and reverse, respectively) 5′-TGAACAGAAGTTAAGGCCAAATATC-3′ and 5′-CAGGCAAAGCTGTAGAATTACATTT-3′ for TGF-β2, 5′-TCCCAGACGAAGACAGTCCCTGGAT-3′ and 5′-CACTGGGGTGGAATGTGTCTTGGTC-3′ for CD44, and 5′-TCCCTGGAGAAGAGCTACGAGC-3′ and 5′-GTAGTTTCGTGGATGCCACAGG-3′ for β-actin (internal control).

EMT-associated Fibrotic Deposits (EAFD) Assay—ARPE-19 cells were cultured in 35-mm dishes for 4 days in the presence of TNF-α or TGF-β2. They were then fixed with methanol for 5 min, air-dried, and stained with Giemsa solution (Merck) for 15 min. The number of EAFDs was counted with the use of a light microscope.

Erythrocyte Exclusion Assay—Fixed sheep red blood cells (Research Diagnostics) were layered onto a monolayer of ARPE-19 cells in a 35-mm dish and incubated for 15 min at room temperature. The cells were then observed with a differential interference contrast (DIC) video microscope (CKX41, Olympus) and analyzed with the use of Flovel software (Olympus).

Cell Binding of Fluorescein-labeled HA—Cells were exposed to fluorescein-labeled HA (Calbiochem) at 100 ng/ml for 6 h, washed with PBS, fixed with 4% paraformaldehyde for 30 min, permeabilized with 0.2% Triton X-100 in PBS for 5 min, and washed with PBS. They were then incubated for 60 min at room temperature with Hoechst 33342 (Invitrogen) diluted in PBS containing 0.2% bovine serum albumin to visualize nuclei. The cells were washed with PBS and examined with a fluorescence microscope (Image Xpress^{MICRO}, Molecular Devices). The average binding of fluorescence-HA to each cell was quantitated with the use of Meta Xpress software.

In Vitro Wound Healing Assay—A sterile plastic micropipette tip was used to make a wound by scratching a monolayer of ARPE-19 cells in serum-free medium. Migration of cells into the wound area was monitored by video microscopy.

RPE Organ Culture System—Mouse retinal organ culture was performed as described (34) with modifications. Mice were killed, and the eyes were enucleated. After removal of the anterior segment and lens and peeling of the retina from each eye, all layers of the posterior eyecup (RPE, choroid, and sclera) were cut into four segments and flattened in the presence of Matrigel (BD Biosciences) on the polyethylene terephthalate membranes (pore size, 0.4 μm) of cell culture inserts (BD Biosciences). The RPE layer adhering to the choroidal sheet was incubated in endothelial basal medium (Lonza) containing hydrocortisone, human epidermal growth factor, bovine brain extract, fetal bovine serum, and antibiotics with or without TNF-α or TGF-β2. The membranes were then removed from the inserts, and the tissue was subjected to immunofluorescence analysis.

In Vivo EMT Model in Mouse Eyes—All animals were treated in accordance with the Association for Research in Vision and Ophthalmology Statement for the Use of Animals in Ophthalmic and Vision Research. C57BL/6J and CD44 knock-out mice (The Jackson Laboratory) at 6–8 weeks of age were anesthetized by intraperitoneal injection of sodium pentobarbital (50 mg/kg) and subjected to injection of TNF-α (400 ng in 2.5 μl of PBS) or PBS (control) into the subretinal region of one eye through the sclera. The injections were performed with a microsyringe (Hamilton) fitted with a sterile 33-gauge needle, with the uninjected contralateral eye serving as a control (35). The mice were killed 14 days after injection, and the eyes were enucleated, fixed with 4% paraformaldehyde, and embedded in paraffin. Sections were cut at a thickness of 4 μm, depleted of paraffin, rehydrated with a graded series of ethanol solutions, and processed for immunofluorescence staining.

RESULTS

EMT-associated Fibrotic Change Results from Interplay between TNF-α and TGF-β2 Signaling in Human RPE Cells—TGF-β is a major inducer of the EMT during embryogenesis, wound healing, fibrotic disorders, and cancer invasion (2, 3). In addition, chronic irritation and inflammation trigger fibrotic disorders (36), and the proinflammatory cytokine TNF-α promotes the EMT cooperatively with TGF-β (37). On the basis of this information, we first investigated the effects of TGF-β and TNF-α on the EMT in cultured epithelial cells. We studied the spontaneously derived human RPE cell line ARPE-19 because of its stable epithelial characteristics, including a cuboidal morphology and the formation of intercellular junctions mediated by N-cadherin in long term culture (38). In retinal pigment epithelial cells, which originate from neural ectoderm, N-cadherin, rather than E-cadherin, is known to behave as dominant cadherin and form stable, zonula adherens-type junctions (39, 40).

TGF-β2 is the major isoform of TGF-β expressed in inflammatory eye diseases (41) and induces fibrotic plaque formation in lens epithelial explants (42). However, exposure to the active form of TGF-β2 alone did not have a marked effect on the morphology of ARPE-19 cells (Fig. 1*A*). In contrast, exposure to TNF-α induced both a pronounced shift in the morphology of ARPE-19 cells to a spindle-like fibroblastic appearance as well as the formation of foci of "piled-up" cells, as revealed by DIC microscopic observation and Giemsa staining of the fixed cells, which allowed us to easily count the number of the cell aggregation (Fig. 1, *A* and *B*). The number of TNF-α-induced cell aggregation was not significantly affected by co-stimulation with TGF-β2 (Fig. 1, *A* and *B*). However, the TNF-α-induced

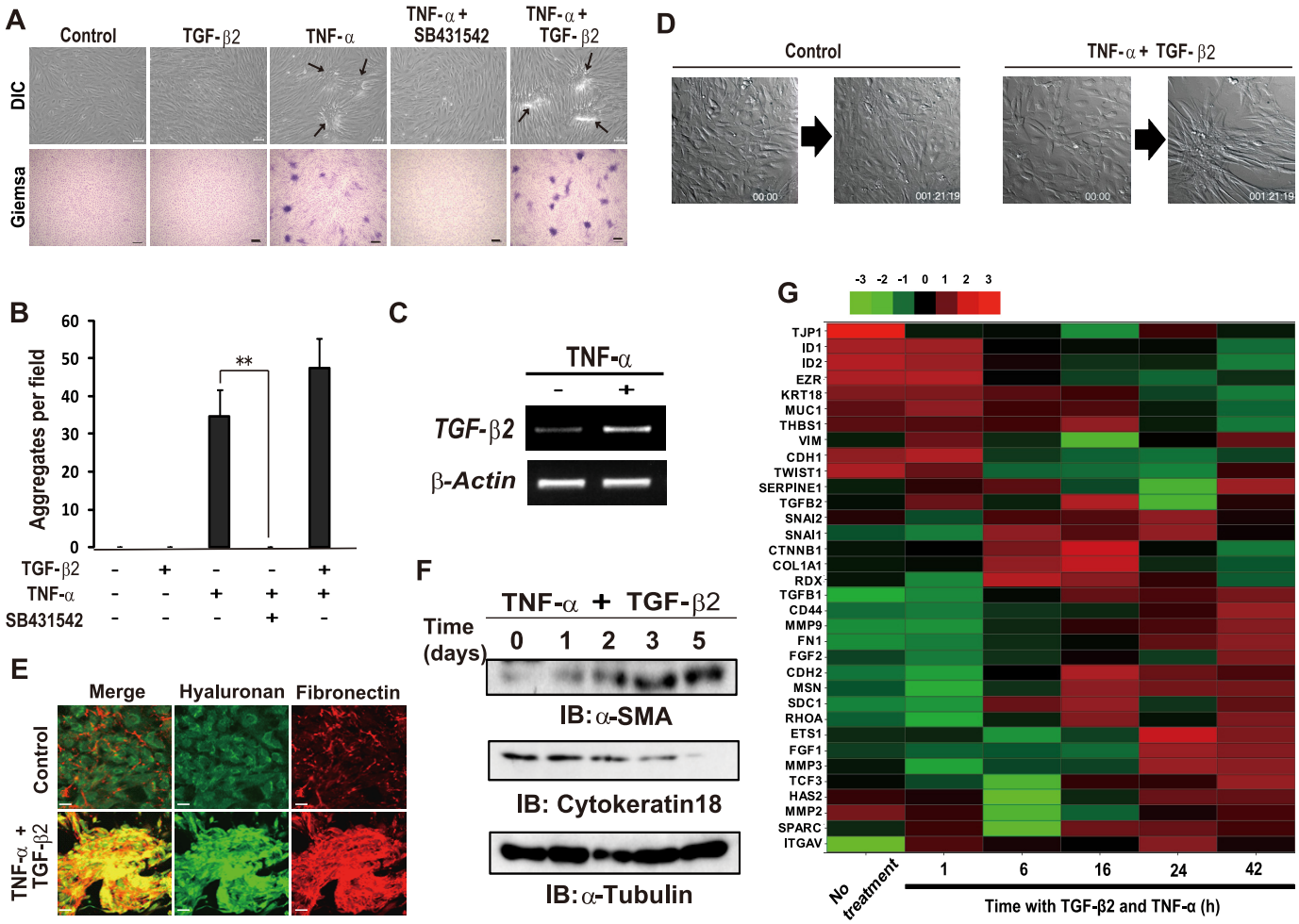

FIGURE 1. **TNF-α and TGF-β2 interdependently promote the formation of EAFDs by ARPE-19 cells.** *A*, confluent cells were cultured for 4 days in the absence (*Control*) or presence of TNF-α (10 ng/ml), TGF-β2 (5 ng/ml), or 10 μM SB431542, an inhibitor of TGF-β receptor I, as indicated. The cells were then either examined by DIC microscopy or fixed and subjected to Giemsa staining. *Arrows* indicate piled-up cell aggregates. *Scale bars*, 100 μm (*upper panels*) or 300 μm (*lower panels*). *B*, the cell aggregates detected by Giemsa staining in experiments shown in *A* were counted by microscopic observation. Data are the means $\pm$ S.D. for 12 different fields in each of three independent experiments. **, $p < 0.01$ (Student's *t* test). *C*, cells were cultured in the absence or presence of TNF-α for 24 h, after which the abundance of TGF-β2 and β-actin (control) mRNAs was determined by RT-PCR analysis. *D*, cells were seeded on glass-bottom plates, incubated in the absence or presence of TNF-α and TGF-β2 in serum-free medium, and observed by time-lapse DIC microscopy (see supplemental Movies 1 and 2). Still images of the cells at times 0 and 45 h 19 min are shown. *E*, confluent cells cultured with or without both TNF-α and TGF-β2 for 48 h were subjected to fluorescence staining with HA binding protein for HA and with antibody to fibronectin. Merged images are also shown. *Scale bars*, 50 μm. *F*, cells were cultured in the presence of both TNF-α and TGF-β2 for the indicated times, after which cell lysates were prepared and subjected to immunoblot analysis (*IB*) with antibodies to α-SMA, cytokeratin 18, or α-tubulin (loading control). *G*, cells were incubated in the absence or presence of both TNF-α and TGF-β2 for the indicated times (hours), after which total RNA was extracted and subjected to microarray analysis. A cluster heat map for EMT-related genes (see supplemental Table 1) is shown. *Red* and *green* denote higher and lower relative expression, respectively; the degree of color saturation reflects the magnitude of the log expression signal according to the indicated scale.

cell aggregation was completely blocked by a specific inhibitor of TGF-β receptor I (SB431542), which acts as a competitive ATP binding site kinase inhibitor and selectively blocks TGF-β signaling but neither bone morphogenic protein signaling nor the extracellular signal-regulated kinase (ERK), p38 mitogen-activated protein kinase (MAPK), and other pathways (43, 44). Furthermore, stimulation with TNF-α alone increased the abundance of TGF-β2 mRNA in ARPE-19 cells (Fig. 1*C*). These results suggested that co-activation of TNF-α and TGF-β2 signaling is necessary for the induction of a fibroblast-like phenotype and the cell aggregation in RPE cells.

To investigate further the phenotypic change induced by TNF-α and TGF-β2 in ARPE-19 cells, we performed time-lapse video microscopy (Fig. 1*D*, supplemental Movies 1 and 2). In contrast to control ARPE-19 cells, which were static and remained in a flat monolayer, cells exposed to both TNF-α and TGF-β2 were highly motile and gathered together to form the piled-up foci. Fluorescence microscopic analysis revealed that the piled-up foci were composed of spindle-shaped cells and various ECM components including HA and fibronectin (Fig. 1*E*) as well as type I collagen and laminin (data not shown). Immunoblot analysis also showed that the combination of TNF-α and TGF-β2 both increased expression of the mesenchymal marker α-SMA as well as down-regulated that of the epithelial marker cytokeratin 18 (Fig. 1*F*). These data, thus, suggested that co-stimulation with TNF-α and TGF-β2 induced the EMT in RPE cells.

To confirm that costimulation with TNF-α and TGF-β2 induces a gene expression profile characteristic of the EMT, we performed cDNA microarray analysis of 47,000 transcripts at

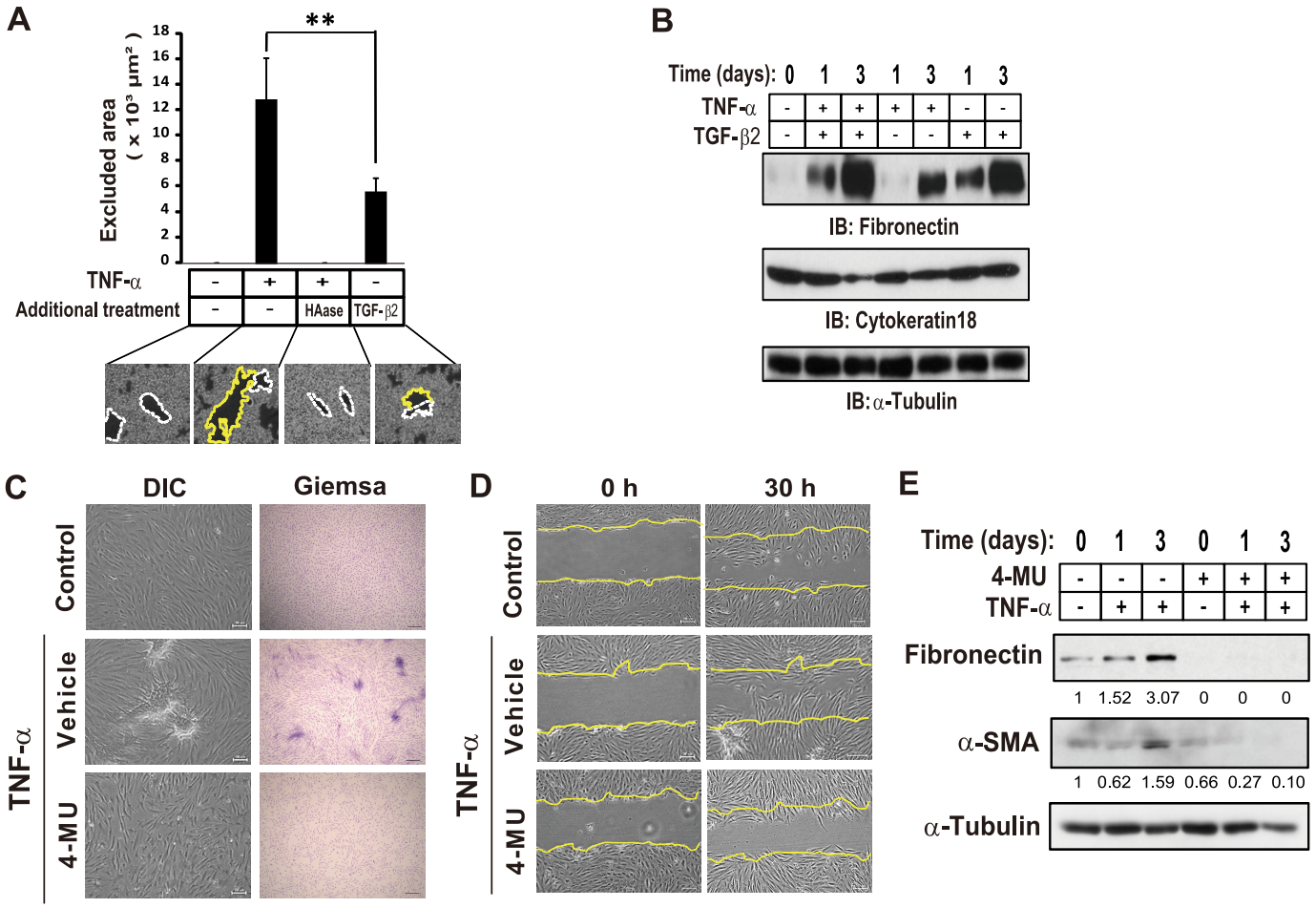

FIGURE 2. **HA synthesis is required for TNF-α-induced EMT in ARPE-19 cells.** *A*, cells were incubated in the absence or presence of TNF-α or TGF-β2 for 24 h. Some cells stimulated with TNF-α were treated with hyaluronidase (10 milliunits/ml) for 1 h before the addition of the fixed erythrocytes. Then the cells were incubated with fixed erythrocytes for 15 min, after which phase-contrast images were obtained (*bottom panels*). Individual cells were traced to determine the cell area (*white dotted lines*), and the external boundary of the halo was traced to determine the area of the pericellular matrix (*yellow lines*). The *area between the two lines* represents the area of the pericellular coat (particle-excluded area) and was expressed as the means ± S.D. for cells in 10 representative fields (*upper panel*). *Scale bar*, 20 μm. **, $p < 0.01$ (Student's *t* test). *B*, cells were cultured in the absence or presence of TNF-α, TGF-β2, or both cytokines for the indicated times, after which cell lysates were prepared and subjected to immunoblot analysis (*IB*) with antibodies to fibronectin, cytokeratin 18, or α-tubulin. *C*, confluent cells were cultured in the absence or presence of the HA synthesis inhibitor 4-MU (1 mM) for 24 h and then in the additional absence or presence of TNF-α for 4 days. The cells were then either examined by DIC microscopy or fixed and subjected to Giemsa staining. *Scale bars*, 100 μm (*left panels*) or 300 μm (*right panels*). *D*, cells exposed to 4-MU as in *C* were cultured in the additional absence or presence of TNF-α for 24 h. The cell monolayer was then scratched, and migration of cells into the wound area was observed at 0 and 30 h thereafter by DIC microscopy. *Yellow lines* indicate the initial margins of the wound. *Scale bars*, 100 μm. *E*, cells exposed to 4-MU as in *C* were cultured in the additional absence or presence of TNF-α for the indicated times, after which cell lysates were prepared and subjected to immunoblot analysis with antibodies to fibronectin, α-SMA, or α-tubulin. *Numbers below each lane* represent the intensity of each band normalized by that of α-tubulin and expressed relative to the normalized value for control cells.

various times after exposure of ARPE-19 cells to the cytokines. As we expected, the expression of EMT-related genes (1, 45) changed in a time-dependent manner (Fig. 1*G*, supplemental Table 1); co-stimulation increased the expression of various mesenchymal type genes, including *SNAI1* (encoding snail), *CD44* (CD44), *MMP9* (matrix metalloproteinase 9), *FN1* (fibronectin), and *COL1A1* (type 1A collagen). Conversely, the expression of key epithelial type genes, such as *TJP1* (tight junction protein 1), *KRT18* (cytokeratin 18), and *CDH1* (E-cadherin), was inhibited by TNF-α and TGF-β2.

Together, our results, thus, suggested that interplay between TNF-α and TGF-β2 signaling induces the EMT in ARPE-19 cells. For subsequent experiments, the characteristic aggregations of ARPE-19 cells induced by these cytokines were termed EAFDs.

HA Synthesis Is Essential for TNF-α-induced EMT in RPE Cells—The ECM microenvironment plays a central role in induction of the EMT. Given that we found that fibronectin and HA were major ECM components of EAFDs (Fig. 1*E*), we investigated which of these components is more important for EMT induction in ARPE-19 cells. We then performed an erythrocyte exclusion assay to visualize the pericellular HA (Fig. 2*A*) and an immunoblot analysis for fibronectin expression in ARPE-19 cells (Fig. 2*B*). In the erythrocyte exclusion assay, a clear zone surrounding cells is generated as a result of exclusion of fixed erythrocytes by the gel-like HA coat (46, 47). Erythrocyte particles were widely excluded from the region surrounding TNF-α-stimulated cells. But the pericellular matrix of TNF-α-stimulated cells was no longer evident after treatment of the cells with hyaluronidase, indicating that HA was the major compo-

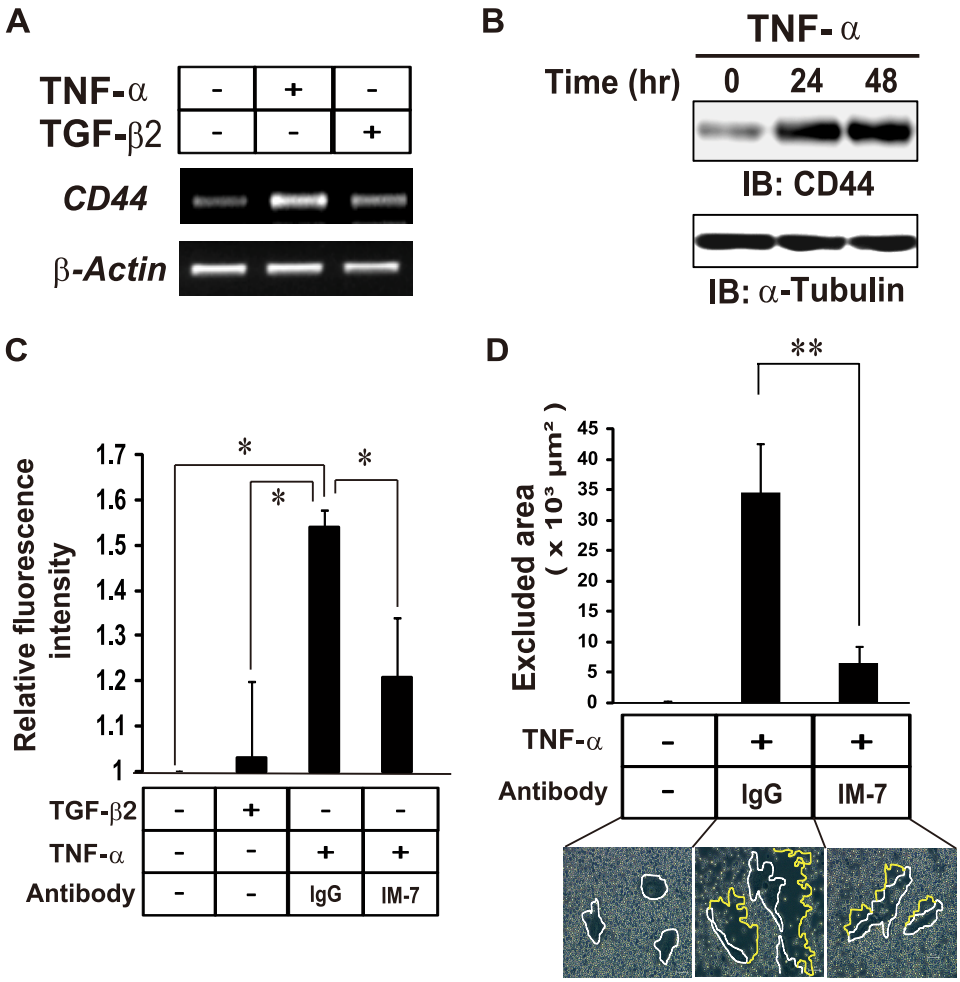

FIGURE 3. **TNF-α promotes HA-CD44 interaction in ARPE-19 cells.** *A*, cells were cultured in the absence or presence of TNF-α or TGF-β2 for 24 h and then subjected to RT-PCR analysis of CD44 or β-actin mRNAs. *B*, cells were cultured in the presence of TNF-α for the indicated times, after which cell lysates were prepared and subjected to immunoblot analysis (*IB*) with antibodies to CD44 or to α-tubulin (loading control). *C*, cells were incubated in the absence or presence of TNF-α or TGF-β2 with or without the IM-7.8.1 antibody to CD44 (20 μg/ml) or control immunoglobulin G (*IgG*) for 24 h and then in the additional presence of fluorescein-HA for 6 h. The binding of fluorescein-HA to the cells was then determined by fluorescence microscopic analysis and expressed relative to the level observed with control cells. Data are the means ± S.D. of values from 12 different fields in each of three independent experiments. *, $p < 0.05$ (Student's *t* test). *D*, cells were cultured for 24 h in the absence or presence of TNF-α and with the IM-7.8.1 antibody to CD44 or control IgG. The cells were then incubated with fixed erythrocytes for 15 min, after which phase-contrast images were obtained (*bottom panels*). The area of the pericellular coat (particle-excluded area) was determined as in Fig. 2*A*. Data are the means ± S.D. for cells in 10 representative fields. *Scale bar*, 20 μm. **, $p < 0.01$ (Student's *t* test).

nent of this pericellular matrix. Importantly, such matrix-dependent erythrocyte exclusion was significantly higher in cells treated with TNF-α than in cells treated with TGF-β2 alone (Fig. 2*A*), whereas TGF-β2 alone could induce slight pericellular matrix formation. In contrast, immunoblot analysis revealed that stimulation with TGF-β2 alone as well as TNF-α alone for 3 days induced the expression of fibronectin (Fig. 2*B*). Although TGF-β2 induced a marked increase in fibronectin expression (Fig. 2*B*), it did not induce EAFD formation (Fig. 1, *A* and *B*). The data raised the possibility that fibronectin does not play a critical role in formation of EMT-associated deposits. Then, to investigate whether HA production is essential for the EMT, we used 4-MU, a well known inhibitor of HA synthesis (48–50). Treatment with 4-MU completely blocked both the induction of EAFD formation (Fig. 2*C*) and the promotion of wound healing *in vitro* (Fig. 2*D*) by TNF-α. Furthermore, 4-MU markedly inhibited the TNF-α-induced expression of mesenchymal markers, α-SMA, and fibronectin (Fig. 2*E*). Given that inhibition of HA synthesis blocked the expression of fibronectin, the possible role of fibronectin in EAFD formation cannot be excluded. However, our findings suggested the importance of HA production in induction of the EMT.

TNF-α Promotes HA-CD44 Interaction in RPE Cells—CD44 is a cell surface receptor for HA and contributes to anchoring of the HA matrix to the cell periphery (6). RT and PCR analysis showed that the amount of *CD44* mRNA in ARPE-19 cells was markedly increased by TNF-α but not by TGF-β2 alone (Fig. 3*A*). The amount of CD44 protein was also increased by TNF-α treatment in a time-dependent manner (Fig. 3*B*). We, therefore, investigated the effect of TNF-α on HA-CD44 interaction in ARPE-19 cells. We first evaluated the ability of cells to bind HA with the use of fluorescein-labeled HA (Fig. 3*C*). The binding of fluorescein-HA to ARPE-19 cells was increased by stimulation of the cells with TNF-α but not by that with TGF-β2. This effect of TNF-α was inhibited by IM-7.8.1, a monoclonal antibody that binds to the extracellular HA binding domain of CD44. Furthermore, the extent of the pericellular HA coat of TNF-α–stimulated cells was significantly reduced in the presence of the IM-7.8.1 monoclonal antibody (Fig. 3*D*). Together, these findings indicate that TNF-α promotes HA-CD44 interaction at the cell surface by the increased level of CD44, leading to pericellular reorganization of HA.

TNF-α Promotes CD44-ERM Interaction through Protein Kinase C (PKC)-dependent Phosphorylation of ERM Proteins—Binding of HA to CD44 is regulated by interaction of the intracellular domain of CD44 with phosphorylated ERM (pERM) in leukocytes (51) and myeloid cells (52). Phosphorylation of ERM proteins is known to be mediated by PKC, p38 MAPK, and Rho kinase (53). We found that TNF-α increased the phosphorylation of ERM proteins in ARPE-19 cells and that such phosphorylation was blocked by a specific inhibitor of PKC (GF109203X) (54) but not by specific inhibitors of p38 MAPK (SB203580) (55) or of Rho kinase (Y-27632) (56) (Fig. 4*A*), suggesting that PKC is responsible for the TNF-α-induced phosphorylation of ERM proteins. Immunocyto-

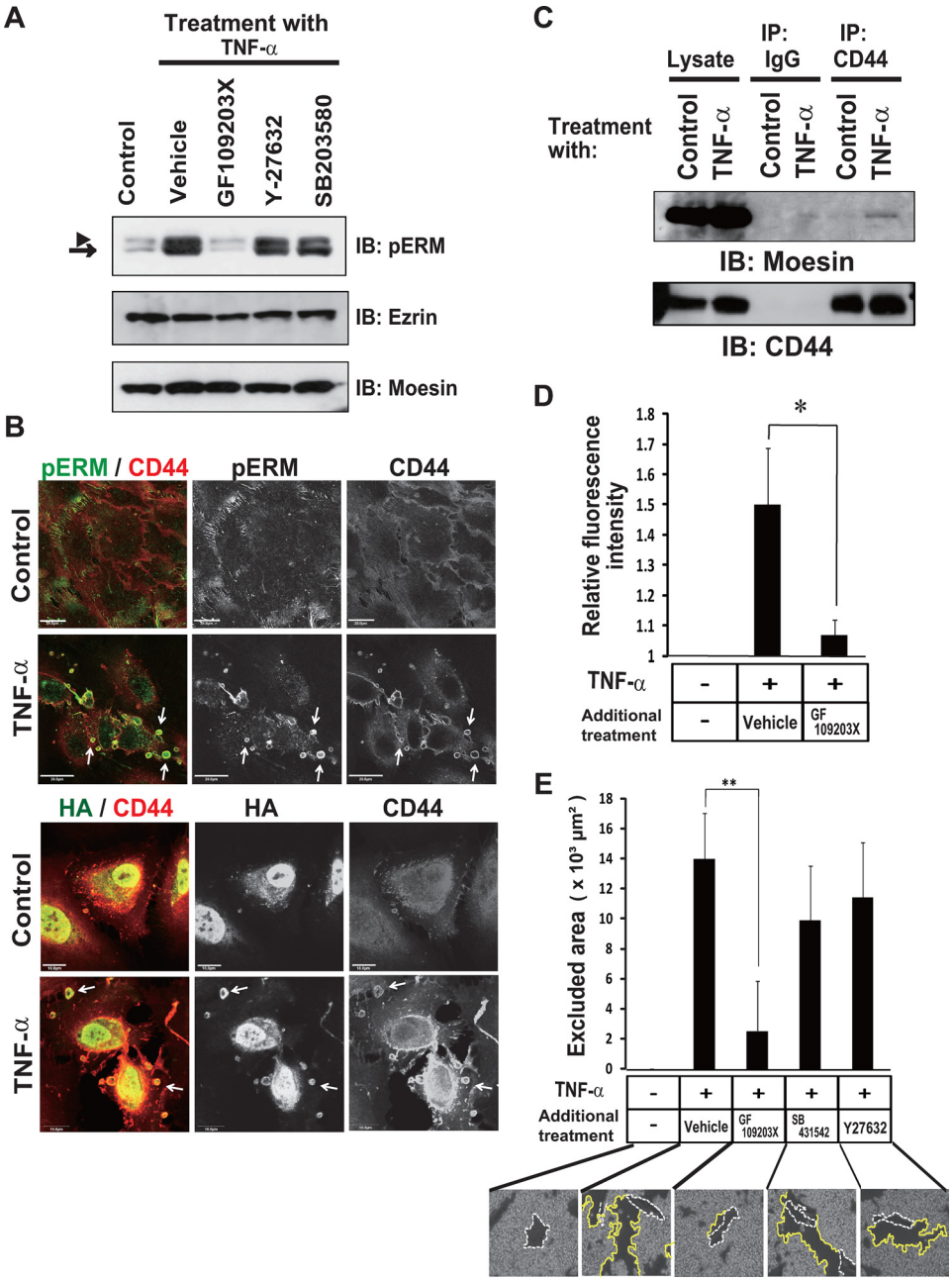

FIGURE 4. **TNF-α induces phosphorylation of ERM and the interaction of ERM with CD44-HA in a PKC-dependent manner in ARPE-19 cells.** *A*, cells were cultured in the absence or presence of TNF-α for 24 h, with the indicated inhibitors GF109203X (2.5 μM), Y-27632 (5 μM), SB203580 (20 μM) added to the medium for the final 3 h. Cell lysates were then prepared and subjected to immunoblot analysis (*IB*) with antibodies to pERM, ezrin, or moesin. The *arrowhead* and *arrow* indicate ezrin-radixin and moesin, respectively. *B*, cells were cultured in the absence or presence of TNF-α for 24 h and then subjected to fluorescence microscopic analysis with antibodies to CD44 and to pERM (*upper panels*) or with antibodies to CD44 and HA binding protein (*lower panels*). *Arrows* indicate colocalization of CD44 and pERM and of CD44 and HA in characteristic spherical extrusions at the cell periphery, respectively. *Scale bars*, 20 μm. It should be noted that HA was also detected in nucleus in both control and TNF-α-treated cells as previously reported (65). *C*, cells cultured in the absence or presence of TNF-α for 24 h were lysed and subjected to immunoprecipitation (*IP*) with antibody to CD44 or with control IgG. The resulting precipitates as well as the cell lysates (2% of the input for immunoprecipitation) were subjected to immunoblot analysis with antibodies to moesin or to CD44. *D*, cells were incubated in the absence or presence of TNF-α with or without GF109203X for 24 h and then in the additional presence of fluorescein-HA for 6 h. The binding of fluorescein-HA to the cells was then determined by fluorescence microscopic analysis and expressed relative to the level observed with control cells. Data are the means ± S.D. of values from 12 different fields in each of three independent experiments. *, $p < 0.05$ (Student's *t* test). *E*, cells were cultured for 24 h in the absence or presence of TNF-α with or without GF109203X, SB431542, or Y-27632. The cells were then incubated with fixed erythrocytes. Phase contrast images were obtained for determination of the area of the pericellular coat (particle-excluded area). Data are the means ± S.D. for cells in 10 representative fields. *Scale bar*, 20 μm. **, $p < 0.01$ (Student's *t* test).

fluorescence analysis revealed that TNF-α induced the colocalization of both pERM and HA with CD44 in characteristic spherical extrusions at the cell periphery (*white arrows*, Fig. 4*B*). Immunoprecipitation analysis confirmed that TNF-α induced the association of the ERM protein moesin with CD44 in ARPE-19 cells (Fig. 4*C*). Furthermore, inhibition of PKC activity with GF109203X blocked both the binding of fluorescein-HA to the cell surface (Fig. 4*D*) and pericellular matrix formation (Fig. 4*E*) induced by TNF-α. Other kinase inhibitors, SB431542 and Y-27632, did not block the HA pericellular matrix formation (Fig. 4*E*). Together, these results indicated that TNF-α-mediated activation of PKC is required for the formation of HA-CD44-phosphorylated moesin complex, which plays a key role in the TNF-α-induced mesenchymal phenotype.

Moesin Is Required for EMT Induction by TNF-α in RPE Cells—CD44-ERM interaction plays a key role in the movement and migratory polarity of cells (57). We, therefore, next examined the effect of TNF-α-induced HA-CD44-ERM interaction on organization of the actin cytoskeleton and cell structure. Untreated ARPE-19 cells manifested radial actin cables and circumferential actin fiber bundles (Fig. 5*A*), both of which are characteristics of epithelial cells. TNF-α induced reorganization of the actin cytoskeleton, with the stimulated cells exhibiting elongated and parallel actin stress fibers similar to those found in fibroblasts (Fig. 5*A*). In addition, cortical actin in dorsal and peripheral areas of the cell body formed spherical extrusions, termed actin microdomains (58), in the TNF-α-treated cells. Furthermore, TNF-α induced the accumulation of pERM to the actin microdomains (Fig. 5*A*). The formation of actin microdomains and the accumulation of pERM to microdomains induced by TNF-α were blocked by the PKC inhibitor GF109203X (Fig. 5*A*). These results, thus, suggested that the PKC-mediated phosphory-

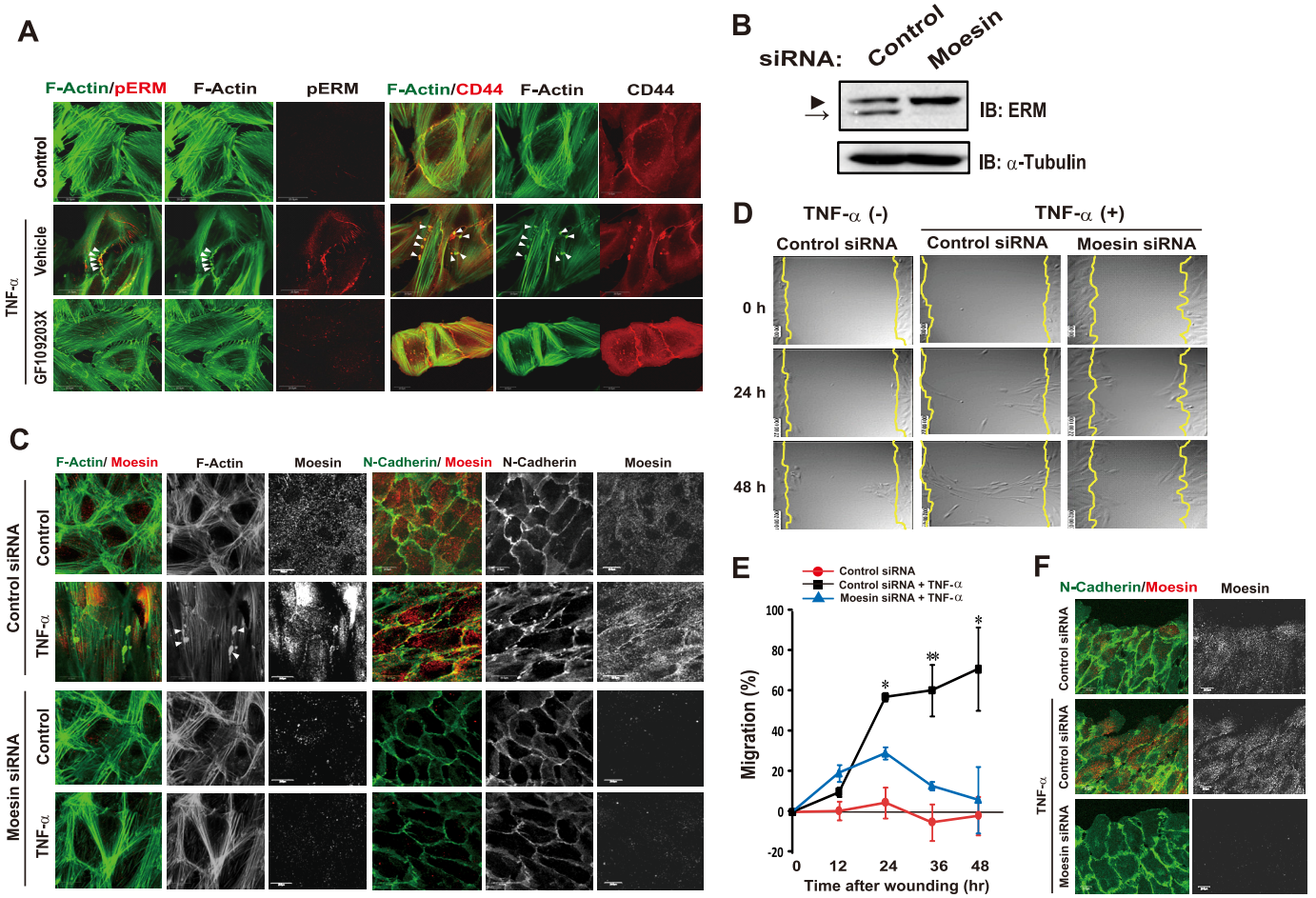

FIGURE 5. **Moesin plays an essential role in TNF-α-induced EMT in ARPE-19 cells.** *A*, cells were cultured for 24 h in the absence or presence of TNF-α or GF109203X, as indicated, and were then subjected to fluorescence microscopic analysis with antibody to pERM and with phalloidin for detection of F-actin (*left panels*) or with antibody to CD44 and with phalloidin (*right panels*). *Arrowheads* indicate actin microdomain formation by TNF-α treatment. *Scale bars*, 20 μm. *B*, lysates of cells transfected with control or moesin siRNAs were subjected to immunoblot analysis (*IB*) with antibodies to ERM or to α-tubulin. The *arrowhead* and *arrow* correspond to ezrin-radixin and moesin, respectively. *C*, cells transfected with control or moesin siRNAs were incubated in the absence or presence of TNF-α for 24 h and then subjected to fluorescence microscopic analysis with antibodies to N-cadherin and moesin and with phalloidin to visualize F-actin. *Arrowheads* indicate actin microdomain formation by TNF-α treatment. *Scale bars*, 20 μm. *D*, cells treated as in *C* were subjected to the *in vitro* wound healing assay as in Fig. 2*C* (see supplemental Movies 3–5). Still images at 0, 24, and 48 h are shown. *E*, quantification of cell migration is shown in *D*. The distance between leading edges of three migrating cells and the wound edge was measured in time-lapse images at the indicated times. Data (% migration) are the means ± S.D. *, $p < 0.05$, **, $p < 0.01$ (Student's *t* test). *F*, cells treated as in *D* for 6 h were subjected to immunofluorescence staining with antibodies to N-cadherin and to moesin.

lation of ERM proteins is required for actin reorganization in cells during the EMT.

The cDNA microarray analysis revealed that among the genes coding ERM proteins, expression of the gene for moesin (*MSN*) was specifically up-regulated during EAFD formation (Fig. 1*G*). Furthermore, moesin itself was prominently phosphorylated in response to TNF-α stimulation in ARPE-19 cells (Fig. 4*A*). We, therefore, next tested the effect of RNAi-mediated moesin depletion (Fig. 5*B*) on EMT induction by TNF-α. TNF-α induced the formation of parallel actin stress fibers and actin microdomains and the disruption of N-cadherin-mediated cell-cell contact in cells treated with a control siRNA (Fig. 5*C*). Whereas moesin-depleted cells showed the epithelial pattern of F-actin and N-cadherin staining under basal conditions, these cells did not manifest the peripheral actin remodeling or disruption of N-cadherin staining at cell-cell boundaries in response to TNF-α stimulation (Fig. 5*C*).

We next examined the contribution of moesin to cell migration with the *in vitro* assay of wound healing. Time-lapse video microscopy revealed that control cells migrated into the wound area en masse, maintaining cell-cell contact during wound closure (Fig. 5, *D–F*, supplemental Movie 3). In contrast, ARPE-19 cells stimulated with TNF-α migrated individually and more rapidly into the wound, continuously changing their orientation and shape (Fig. 5, *D–F*, supplemental Movie 4). These effects of TNF-α were markedly inhibited in cells depleted of moesin by RNAi (Fig. 5, *D–F*, supplemental Movie 5). Overall, these data indicated that moesin plays an essential role in the induction by TNF-α of phenotypes associated with the EMT in RPE cells.

TNF-α-induced CD44 Expression Reinforces TGF-β-dependent EMT—As mentioned above, we found that both TNF-α and TGF-β are necessary for EMT induction in ARPE-19 cells. In addition, TNF-α was shown to promote HA·CD44·pERM interaction at the cell periphery, with such interaction being a key event in EMT induction. We, therefore, examined whether CD44 is required for the activation of TGF-β signaling in ARPE-19 cells. HA-CD44 interaction was previously shown to

stimulate the serine-threonine kinase activity of the TGF-β receptor and thereby to induce phosphorylation of Smad2/3 through the association of CD44 with the TGF-β receptor (59). Furthermore, it has been shown that clathrin-dependent internalization of TGF-β receptors promotes TGF-β signaling through Smad2 activation, whereas the lipid raft-caveolar

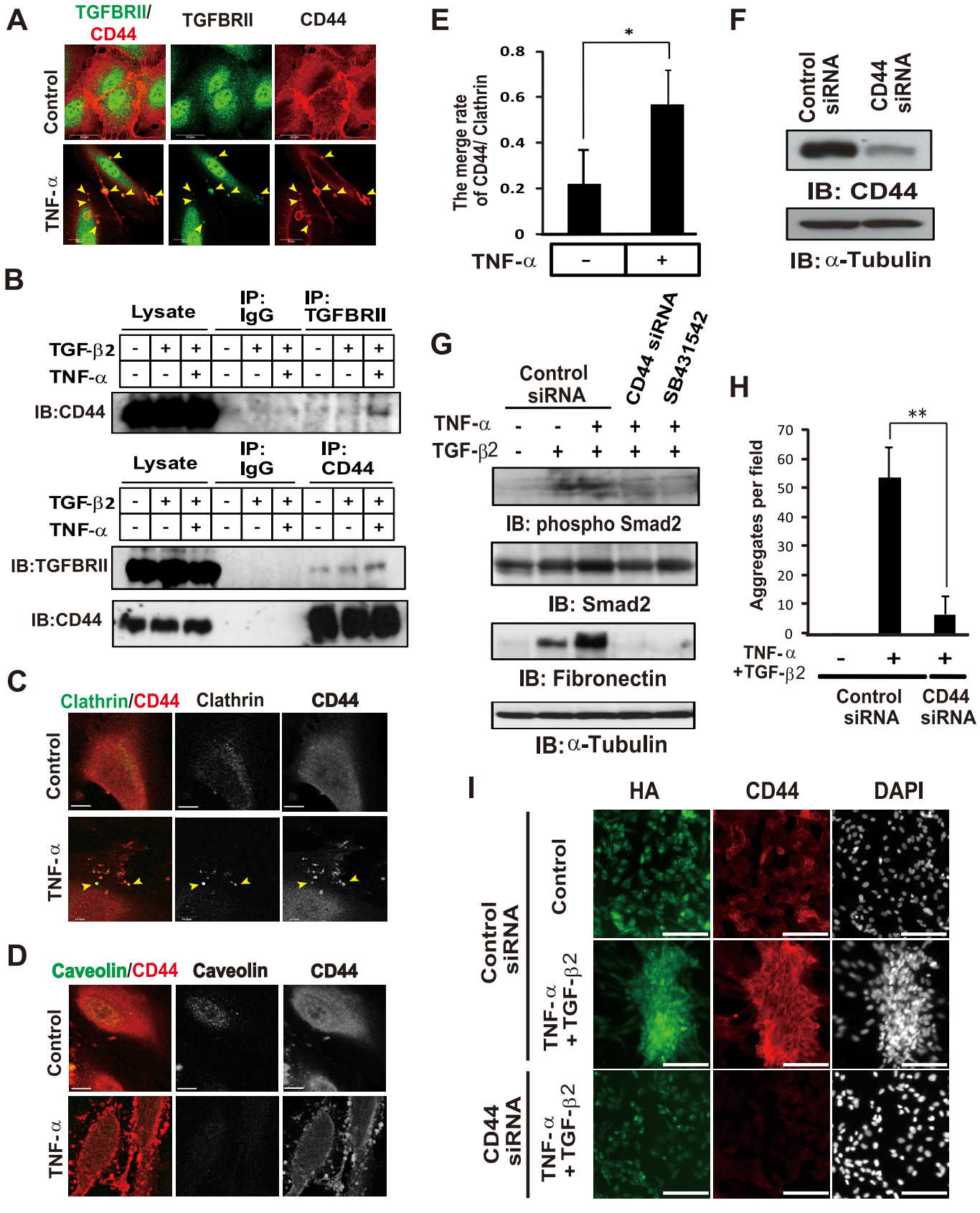

internalization pathway promotes rapid receptor turnover, leading to inactivation of TGF-β signaling (60). Based on this knowledge, we attempted to investigate the interaction of CD44 with TGF-β receptor II. Immunocytofluorescence analysis showed that CD44 colocalized with endogenous TGF-β receptor II at actin microdomains in TNF-α–stimulated ARPE-19 cells (Fig. 6*A*). Furthermore, immunoprecipitation analysis showed that the stimulation with TNF-α plus TGF-β promotes the association of CD44 with TGF-β receptor II (Fig. 6*B*). Additionally, CD44-positive spots were colocalized with clathrin but not with caveolin in TNF-α-treated cells (Fig. 6, *C* and *D*). Although the merge rate of CD44- and clathrin-positive spots was significantly increased by TNF-α treatment (Fig. 6*E*), the expression of caveolin was decreased in the presence of TNF-α (not shown). These data suggested that CD44 is involved in TGF-β activation in the presence of TNF-α. In fact, the induction by TNF-α and TGF-β2 of Smad2 phosphorylation and fibronectin expression, both of which are important downstream events in TGF-β signaling, was suppressed by RNAi-mediated depletion of CD44 as well as by treatment with SB431542, an inhibitor of the TGF-β type I receptor (Fig. 6, *F* and *G*). These findings suggested that CD44 is required for the activation of TGF-β signaling in ARPE-19 cells.

We also examined the effect of CD44 depletion on the EMT-mediated EAFD formation. Treatment with TNF-α and TGF-β2 induced aggregation of cells with accumulation of HA and high expression of CD44 (Fig. 6, *H* and *I*). However, CD44 depletion significantly blocked the HA-rich EAFD formation, suggesting that CD44-mediated signal reinforces the activation of TGF-β pathway during induction of the EMT.

TNF-α-induced and CD44-mediated Acquisition of the Mesenchymal Phenotype Results in Fibrosis in the Mouse Eye—We next examined the requirement for CD44 in TNF-α-induced EMT with the use of a mouse RPE organ culture system. The RPE layer adhering to the choroidal sheet was spread flat and cultured in endothelial basal medium in the absence or presence of TNF-α or TGF-β2 (Fig. 7*A*). Immunostaining for N-cadherin revealed the typical hexagonal shape of RPE cells in the control culture condition (Fig. 7*B*). Exposure of RPE cells to TGF-β2 did not affect the hexagonal pattern of N-cadherin staining, whereas treatment with TNF-α resulted in disruption of N-cadherin-mediated cell-cell contacts (Fig. 7*B*). Furthermore, exposure of RPE cells in long-term organ culture to TNF-α resulted in their adoption of a fibroblastic morphology and formation of HA-rich piled-up structures (Fig. 7*C*). In contrast, TNF-α did not affect the epithelial morphology of, or the localization of N-cadherin at sites of cell-cell contact in RPE cells prepared from CD44 knock-out mice. Furthermore, the TNF-α-induced accumulation of HA was not detected with the RPE cells from CD44 knock-out mice (Fig. 7*C*).

Finally, we established a model of TNF-α-induced fibrosis in the mouse eye. When PBS was injected into the subretinal region of the mouse eye, RPE cells repaired the wound while maintaining their epithelial phenotype on Bruch's membrane (Fig. 7*D*). In contrast, when TNF-α was injected instead of PBS, the injured RPE cells formed multiple layers, with dense fibrous tissue composed of elongated fibroblast-like cells apparent at day 14. These cells expressed α-SMA at a high level, a hallmark of mesenchymal cells, as well as manifested up-regulation of CD44 (Fig. 7, *D* and *E*). In CD44 knock-out mice, RPE cells did not become elongated or form fibrous tissue in response to injection of TNF-α but, rather, behaved as did those in wild-type mice injected with PBS (Fig. 7, *D* and *E*). These findings, thus, indicated that CD44 plays a key role in the development of fibrosis associated with TNF-α-induced EMT *in vivo*.

DISCUSSION

During embryonic development and normal wound healing, the EMT is tightly regulated by "on" and "off" switches. However, the balance between the EMT and the reverse transition is thought to become deregulated in pathological conditions such as chronic inflammation, favoring the EMT. Cells that have undergone the EMT under such conditions produce excess amounts of ECM and aggregate at sites of inflammation, resulting in the development of fibrosis (2, 20, 61).

We have now provided evidence from both *in vitro* and *in vivo* models that the proinflammatory cytokine TNF-α plays a key role in the induction of fibrosis associated with the mesenchymal change of RPE cells. EMT-associated fibrosis was, thus, found to be induced by activation of TGF-β signaling as a result of HA-CD44-ERM interaction promoted by TNF-α (Fig. 8). Our findings provide both insight into the mechanism underlying the relation between chronic inflammation and the EMT as well as a basis for the development of new therapeutic strategies to avert fibrotic disorders.

TNF-α Activates TGF-β Signaling for Induction of EMT in RPE Cells—We studied EAFD formation as an indicator of EMT-associated fibrotic reactions in RPE cells. The formation of EAFDs appeared to result from the combination of ECM

FIGURE 6. **TNF-α-induced interaction of CD44 with TGF-β receptor II is essential for TGF-β-dependent EMT.** *A*, cells cultured with or without TNF-α for 48 h were subjected to immunofluorescence staining with antibodies to TGF-β receptor II and to CD44. *Yellow arrowheads* indicate the colocalization of TGF-β receptor II (*TGFBRII*) and CD44 in ARPE-19 cells treated with TFN-α. *Scale bars*, 20 μm. *B*, cells cultured with or without TFN-α for 48 h and TGF-β2 for the last 15 min were lysed and subjected to immunoprecipitation (*IP*) with antibodies to TGF-β receptor II or to CD44 or with control IgG. The resulting precipitates as well as the whole cell lysates were subjected to immunoblot (*IB*) analysis with antibodies to TGF-β receptor II or to CD44. *C*, cells cultured with or without TNF-α for 48 h were stained with antibodies to clathrin and to CD44. *Yellow arrowheads* indicate the colocalization of clathrin and CD44 in ARPE-19 cells treated with TFN-α. *Scale bars*, 10 μm. *D*, cells cultured with or without TNF-α for 48 h were stained with antibodies to caveolin and to CD44. Caveolin did not colocalize to CD44. *Scale bars*, 20 μm. *E*, The ratio of clathrin-positive spots merged with CD44-positive spots was counted after the immunofluorescence staining of ARPE-19 cells treated with or without TNF-α. Data are means $\pm$ S.D. for cells in three representative fields. *$p < 0.05$ (Student's *t* test). *F*, lysates of cells transfected with control or CD44 siRNAs were subjected to immunoblot analysis with antibodies to CD44 or to α-tubulin. *G*, cells transfected with control or CD44 siRNAs were incubated in the absence or presence of TNF-α, TGF-β2, or SB431542 for 48 h, after which cell lysates were prepared and subjected to immunoblot analysis with antibodies to phosphorylated or total forms of Smad2, fibronectin, or α-tubulin. *H*, cells transfected with control or CD44 siRNAs were incubated in the absence or presence of both TNF-α and TGF-β2 for 48 h, fixed, and subjected to Giemsa staining for determination of the number of EAFDs. Data are the means $\pm$ S.D. for 12 different fields in each of three independent experiments. **, $p < 0.01$ (Student's *t* test). *I*, cells treated as in *H* were subjected to immunofluorescence staining with antibodies to CD44, HA binding protein, and 4′,6-diamidino-2-phenylindole (*DAPI*, for nuclei). *Scale bars*, 100 μm.

overproduction and migration of the fibroblast-like cells within the ECM deposit. EAFD formation, thus, provides an *in vitro* model of fibrotic disorders. We found that TNF-α or the combination of TNF-α and TGF-β2 induced EAFD formation. Whereas TGF-β2 alone was able to increase the expression of certain mesenchymal markers such as fibronectin as well as to induce small morphologic changes in RPE cells, it was not sufficient to induce EAFD formation. However, we found that

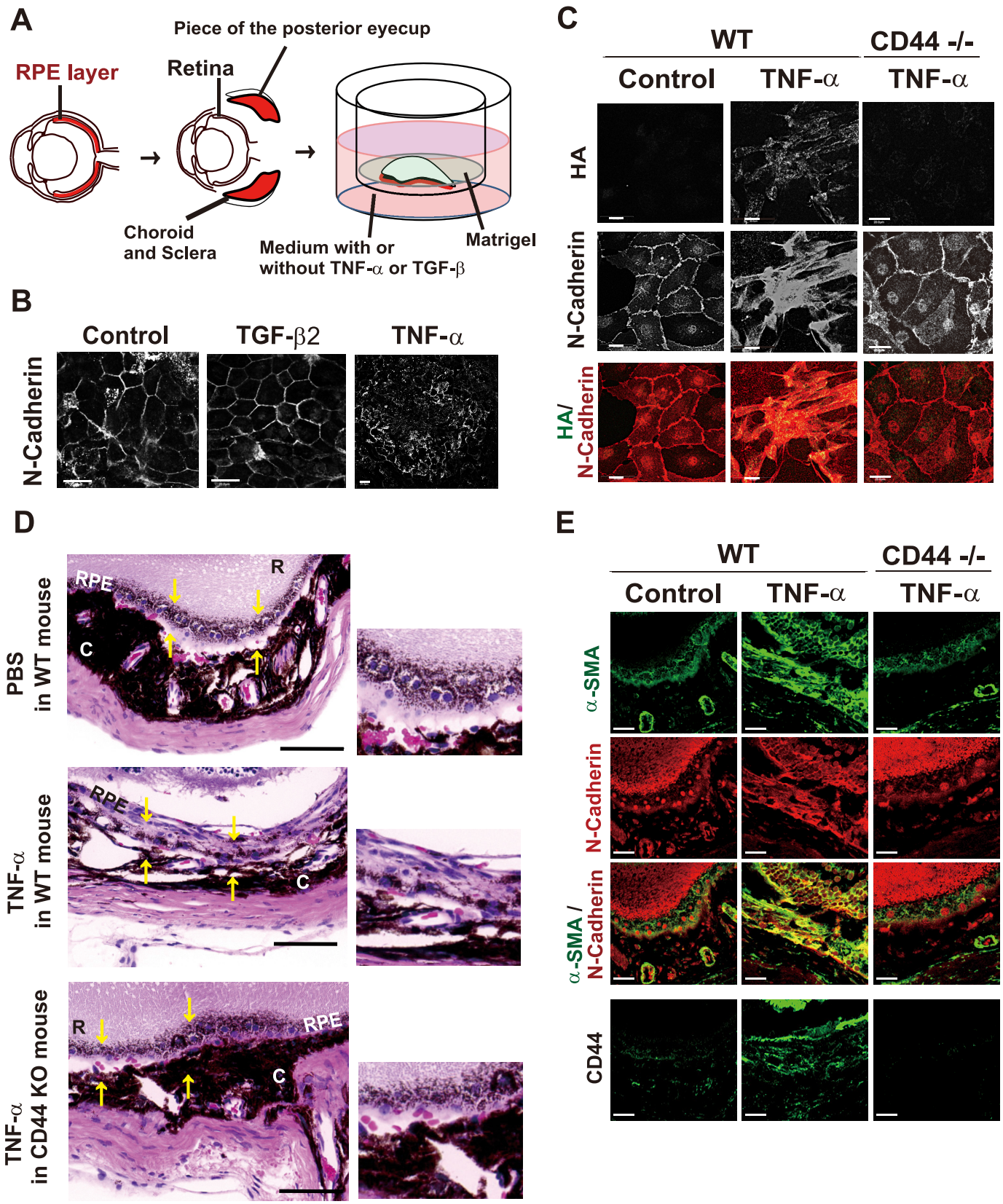

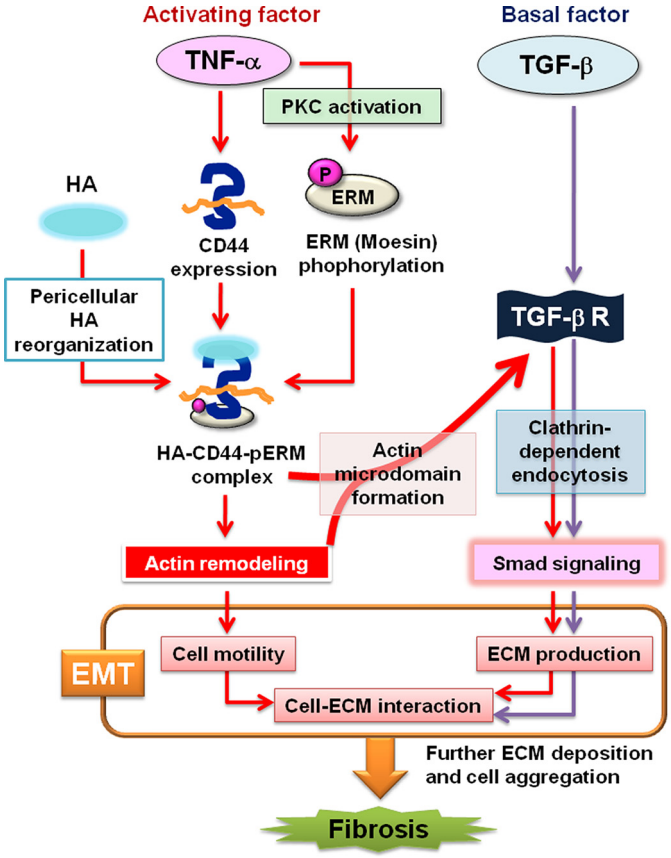

FIGURE 8. **Model of the signaling pathways underlying TNF-α-induced EMT.** TNF-α induces the expression of CD44 and the phosphorylation of ERM in a manner dependent on PKC activation and thereby promotes formation of the HA·CD44·pERM complex. This complex then triggers remodeling of the actin cytoskeleton and the CD44-TGF-β receptor interaction, leading to the activation of Smad signaling through TGF-β receptor clustering and EMT induction. Persistent activation of EMT results in fibrotic disorder.

TNF-α induced *TGF-β2* gene expression and that the activation of TGF-β receptors was essential for TNF-α-induced EMT and EAFD formation. Persistent stimulation with TNF-α, which mimics inflammatory conditions, thus appears to activate TGF-β signaling, leading to fibrotic reactions as a result of deviation from the balance between the EMT and the reverse transition.

TNF-α Promotes the Formation of HA·CD44·pERM Complex through PKC Activation—The ECM component HA and its biosynthetic enzymes (HASs) have been implicated in the EMT associated with cardiac development (8) and various fibrotic disorders. Indeed, our present results show that pericellular interaction between HA and CD44 is necessary for TNF-α-induced EAFD formation and wound healing *in vitro*. However, the mechanism by which HA contributes to the EMT has remained unknown. We have now shown that CD44 expression is increased by TNF-α and that subsequent formation of the membrane-spanning HA·CD44·pERM complex is required for induction and maintenance of the EMT.

Activation of PKC was found to be a key step in formation of the HA·CD44·pERM complex. Previous studies have shown that TNF-α activates PKC (62) and that PKC activation promotes HA synthesis by HAS (63). We now show that TNF-α stimulation promotes association of HA with CD44 at the cell periphery and that this association is accompanied by the interaction of CD44 with pERM, in particular with phosphorylated moesin. Formation of the HA·CD44·pERM complex appears to promote a switch from cell-cell contact to cell-HA interaction through remodeling of the actin cytoskeleton. The phosphorylation of ERM proteins was mediated by PKC in response to TNF-α stimulation. Our results, thus, indicate that activation of PKC by TNF-α promotes the phosphorylation of ERM proteins, facilitating formation of the HA·CD44·pERM complex at the plasma membrane.

HA·CD44·pERM Complex Is Required for Activation of TGF-β Signaling—Several lines of evidence provide support for the notion that TNF-α activates TGF-β signaling by promoting formation of the HA·CD44·pERM complex. Clathrin-dependent internalization of TGF-β receptors into EEA1-positive endosomes, in which the Smad2 anchor SARA is enriched, has previously been shown to activate TGF-β signaling (60). In contrast, the caveolin-dependent internalization of TGF-β promotes rapid receptor turnover, leading to inactivation of TGF-β signaling. Our results indicate that TNF-α-induced formation of the membrane-spanning HA·CD44·pERM complex resulted in reorganization of the actin cytoskeleton and promoted the formation of actin microdomains, which spatially organize signaling molecules at the membrane. Such CD44-positive microdomains were associated with TGF-β receptor II and clathrin but not with caveolin-1. Therefore, the clustering of TGF-β receptors at actin microdomains may result in activation of TGF-β signaling. It is, thus, possible that cells with preexisting HA·CD44·pERM complexes may be induced to undergo EMT-associated fibrotic reactions by TGF-β stimulation alone (in the absence of TNF-α).

TGF-β is usually released from cells in a latent form that must be proteolytically processed to yield the biologically active form. This activation of TGF-β was recently shown to be dependent on CD44 and to be mediated by a matrix metalloproteinase (64). Such a mechanism cannot explain our findings

FIGURE 7. **TNF-α-induced acquisition of the mesenchymal phenotype mediated by CD44 results in fibrosis in the mouse eye.** *A*, shown is the experimental system for RPE culture. Pieces of the posterior eyecup with the retina removed were flattened (RPE layer down) by Matrigel onto a cell culture insert and then incubated with culture medium in the lower chamber containing (or not) TNF-α (10 ng/ml) or TGF-β2 (5 ng/ml). *B*, tissue incubated as in *A* with or without TNF-α or TGF-β2 for 3 days was fixed and subjected to immunofluorescence staining with antibody to N-cadherin. *Scale bars*, 20 μm. *C*, tissue from wild-type (*WT*) or CD44 knock-out (*CD44*$^{-/-}$) mouse littermates was incubated as in *A* in the absence or presence of TNF-α for 7 days, fixed, and subjected to fluorescence microscopic analysis with HA binding protein and antibody to N-cadherin. Merged images show HA in *green* and N-cadherin in *red*. *Scale bars*, 20 μm. *D*, TNF-α or PBS was injected into the subretinal layer of CD44 knock-out (*KO*) or wild-type mouse littermates. Eyes were enucleated 14 days after injection, fixed, and embedded in paraffin. Sections were then prepared and stained with hematoxylin-eosin. Areas demarcated by *yellow arrows* indicate the RPE at the site of the injection (*left panels*). *R*, retina; *C*, choroid. *Scale bars*, 80 μm. Higher magnification images of the demarcated areas are shown in the *right panels*. *E*, sections of eyes treated as in *D* were subjected to immunofluorescence staining with antibodies to α-SMA, N-cadherin, and CD44. *Scale bars*, 50 μm. *WT*, wild type.

with TGF-β, however, because we used the active form of TGF-β2 in our experiments. CD44 may, thus, play dual roles in the activation of TGF-β signaling by promoting the extracellular conversion of the latent form of TGF-β to the active form and by inducing the intracellular activation of the Smad-dependent signaling pathway.

In summary, we have shown that TNF-α and TGF-β cooperatively induce the EMT and that formation of the HA·CD44·pERM complex in a manner dependent on PKC activation is an important step in TNF-α action, leading to loss of cell-cell contact, changes in cell morphology, and ECM overproduction. Both our RPE organ culture and subretinal injection experiments also showed that TNF-α induces EMT-associated fibrosis in the RPE in a manner dependent on CD44. The interactions among HA, CD44, and ERM proteins, in particular moesin, thus represent potential targets for the development of new therapeutic agents for the treatment of EMT-associated pathological states such as fibrosis and inflammation as well as tumor invasion and metastasis.

Acknowledgments—We thank I. Ishimatsu and N. Suzuki for technical assistance as well as K. Arai for secretarial assistance. We thank O. Sampetrean and S. H. Lee for critical discussions.

REFERENCES

1. Lee, J. M., Dedhar, S., Kalluri, R., and Thompson, E. W. (2006) *J. Cell Biol.* **172,** 973–981
2. Thiery, J. P. (2002) *Nat. Rev. Cancer* **2,** 442–454
3. Kalluri, R., and Neilson, E. G. (2003) *J. Clin. Invest.* **112,** 1776–1784
4. Zuk, A., Matlin, K. S., and Hay, E. D. (1989) *J. Cell Biol.* **108,** 903–919
5. Shintani, Y., Wheelock, M. J., and Johnson, K. R. (2006) *Mol. Biol. Cell* **17,** 2963–2975
6. Laurent, T. C., and Fraser, J. R. (1992) *FASEB J.* **6,** 2397–2404
7. Itano, N., Sawai, T., Yoshida, M., Lenas, P., Yamada, Y., Imagawa, M., Shinomura, T., Hamaguchi, M., Yoshida, Y., Ohnuki, Y., Miyauchi, S., Spicer, A. P., McDonald, J. A., and Kimata, K. (1999) *J. Biol. Chem.* **274,** 25085–25092
8. Camenisch, T. D., Spicer, A. P., Brehm-Gibson, T., Biesterfeldt, J., Augustine, M. L., Calabro, A., Jr., Kubalak, S., Klewer, S. E., and McDonald, J. A. (2000) *J. Clin. Invest.* **106,** 349–360
9. Zeng, C., Toole, B. P., Kinney, S. D., Kuo, J. W., and Stamenkovic, I. (1998) *Int. J. Cancer* **77,** 396–401
10. Ghatak, S., Misra, S., and Toole, B. P. (2002) *J. Biol. Chem.* **277,** 38013–38020
11. Rodgers, L. S., Lalani, S., Hardy, K. M., Xiang, X., Broka, D., Antin, P. B., and Camenisch, T. D. (2006) *Circ. Res.* **99,** 583–589
12. Ponta, H., Sherman, L., and Herrlich, P. A. (2003) *Nat. Rev. Mol. Cell Biol.* **4,** 33–45
13. Nagano, O., and Saya, H. (2004) *Cancer Sci.* **95,** 930–935
14. Haynes, B. F., Hale, L. P., Patton, K. L., Martin, M. E., and McCallum, R. M. (1991) *Arthritis Rheum.* **34,** 1434–1443
15. Kuppner, M. C., Liversidge, J., McKillop-Smith, S., Lumsden, L., and Forrester, J. V. (1993) *Curr. Eye Res.* **12,** 923–934
16. Florquin, S., Nunziata, R., Claessen, N., van den Berg, F. M., Pals, S. T., and Weening, J. J. (2002) *Am. J. Kidney Dis.* **39,** 407–414
17. Svee, K., White, J., Vaillant, P., Jessurun, J., Roongta, U., Krumwiede, M., Johnson, D., and Henke, C. (1996) *J. Clin. Invest.* **98,** 1713–1727
18. Teder, P., Vandivier, R. W., Jiang, D., Liang, J., Cohn, L., Puré, E., Henson, P. M., and Noble, P. W. (2002) *Science* **296,** 155–158
19. Rouschop, K. M., Sewnath, M. E., Claessen, N., Roelofs, J. J., Hoedemaeker, I., van der Neut, R., Aten, J., Pals, S. T., Weening, J. J., and Florquin, S. (2004) *J. Am. Soc. Nephrol.* **15,** 674–686
20. Noble, P. W., and Jiang, D. (2006) *Proc. Am. Thorac. Soc.* **3,** 401–404
21. Limb, G. A., Chignell, A. H., Woon, H., Green, W., Cole, C. J., and Dumonde, D. C. (1996) *Graefes Arch. Clin. Exp. Ophthalmol.* **234,** 213–220
22. Casaroli-Marano, R. P., Pagan, R., and Vilaró, S. (1999) *Invest. Ophthalmol. Vis. Sci.* **40,** 2062–2072
23. Campochiaro, P. A. (1997) *Arch. Ophthalmol.* **115,** 237–241
24. Lei, H., Hovland, P., Velez, G., Haran, A., Gilbertson, D., Hirose, T., and Kazlauskas, A. (2007) *Invest. Ophthalmol. Vis. Sci.* **48,** 2335–2342
25. Agrawal, R. N., He, S., Spee, C., Cui, J. Z., Ryan, S. J., and Hinton, D. R. (2007) *Nat. Protoc.* **2,** 67–77
26. Armstrong, D., Augustin, A. J., Spengler, R., Al-Jada, A., Nickola, T., Grus, F., and Koch, F. (1998) *Ophthalmologica* **212,** 410–414
27. Wiedemann, P. (1992) *Surv. Ophthalmol.* **36,** 373–384
28. Bourguignon, L. Y., Singleton, P. A., Diedrich, F., Stern, R., and Gilad, E. (2004) *J. Biol. Chem.* **279,** 26991–27007
29. Hirota, T., Kunitoku, N., Sasayama, T., Marumoto, T., Zhang, D., Nitta, M., Hatakeyama, K., and Saya, H. (2003) *Cell* **114,** 585–598
30. Nagano, O., Murakami, D., Hartmann, D., De Strooper, B., Saftig, P., Iwatsubo, T., Nakajima, M., Shinohara, M., and Saya, H. (2004) *J. Cell Biol.* **165,** 893–902
31. Cheadle, C., Vawter, M. P., Freed, W. J., and Becker, K. G. (2003) *J. Mol. Diagn.* **5,** 73–81
32. Kerr, M. K., Martin, M., and Churchill, G. A. (2000) *J. Comput. Biol.* **7,** 819–837
33. Okamoto, I., Morisaki, T., Sasaki, J., Miyake, H., Matsumoto, M., Suga, M., Ando, M., and Saya, H. (1998) *J. Natl. Cancer Inst.* **90,** 307–315
34. Mitsuda, S., Yoshii, C., Ikegami, Y., and Araki, M. (2005) *Dev. Biol.* **280,** 122–132
35. Dureau, P., Legat, L., Neuner-Jehle, M., Bonnel, S., Pecqueur, S., Abitbol, M., and Dufier, J. L. (2000) *Graefes Arch. Clin. Exp. Ophthalmol.* **238,** 608–614
36. Kalluri, R., and Zeisberg, M. (2006) *Nat. Rev. Cancer* **6,** 392–401
37. Bates, R. C., and Mercurio, A. M. (2003) *Mol. Biol. Cell* **14,** 1790–1800
38. Inumaru, J., Nagano, O., Takahashi, E., Ishimoto, T., Nakamura, S., Suzuki, Y., Niwa, S., Umezawa, K., Tanihara, H., and Saya, H. (2009) *Genes Cells* **14,** 703–716
39. McKay, B. S., Irving, P. E., Skumatz, C. M., and Burke, J. M. (1997) *Exp. Eye Res.* **65,** 661–671
40. Kaida, M., Cao, F., Skumatz, C. M., Irving, P. E., and Burke, J. M. (2000) *Invest. Ophthalmol. Vis. Sci.* **41,** 3215–3224
41. Connor, T. B., Jr., Roberts, A. B., Sporn, M. B., Danielpour, D., Dart, L. L., Michels, R. G., de Bustros, S., Enger, C., Kato, H., and Lansing, M. (1989) *J. Clin. Invest.* **83,** 1661–1666
42. Banh, A., Deschamps, P. A., Vijayan, M. M., Sivak, J. G., and West-Mays, J. A. (2007) *Mol. Vis.* **13,** 2248–2262
43. Callahan, J. F., Burgess, J. L., Fornwald, J. A., Gaster, L. M., Harling, J. D., Harrington, F. P., Heer, J., Kwon, C., Lehr, R., Mathur, A., Olson, B. A., Weinstock, J., and Laping, N. J. (2002) *J. Med. Chem.* **45,** 999–1001
44. Inman, G. J., Nicolás, F. J., Callahan, J. F., Harling, J. D., Gaster, L. M., Reith, A. D., Laping, N. J., and Hill, C. S. (2002) *Mol. Pharmacol.* **62,** 65–74
45. Zavadil, J., Bitzer, M., Liang, D., Yang, Y. C., Massimi, A., Kneitz, S., Piek, E., and Bottinger, E. P. (2001) *Proc. Natl. Acad. Sci. U.S.A.* **98,** 6686–6691
46. Knudson, C. B., and Knudson, W. (1993) *FASEB J.* **7,** 1233–1241
47. Lee, G. M., Johnstone, B., Jacobson, K., and Caterson, B. (1993) *J. Cell Biol.* **123,** 1899–1907
48. Kosaki, R., Watanabe, K., and Yamaguchi, Y. (1999) *Cancer Res.* **59,** 1141–1145
49. Sohara, Y., Ishiguro, N., Machida, K., Kurata, H., Thant, A. A., Senga, T., Matsuda, S., Kimata, K., Iwata, H., and Hamaguchi, M. (2001) *Mol. Biol. Cell* **12,** 1859–1868
50. Rilla, K., Pasonen-Seppänen, S., Rieppo, J., Tammi, M., and Tammi, R. (2004) *J. Invest. Dermatol.* **123,** 708–714
51. Maiti, A., Maki, G., and Johnson, P. (1998) *Science* **282,** 941–943
52. Brown, K. L., Birkenhead, D., Lai, J. C., Li, L., Li, R., and Johnson, P. (2005) *Exp. Cell Res.* **303,** 400–414
53. Koss, M., Pfeiffer, G. R., 2nd, Wang, Y., Thomas, S. T., Yerukhimovich, M.,

Gaarde, W. A., Doerschuk, C. M., and Wang, Q. (2006) *J. Immunol.* **176,** 1218–1227
54. Toullec, D., Pianetti, P., Coste, H., Bellevergue, P., Grand-Perret, T., Ajakane, M., Baudet, V., Boissin, P., Boursier, E., and Loriolle, F. (1991) *J. Biol. Chem.* **266,** 15771–15781
55. Tong, L., Pav, S., White, D. M., Rogers, S., Crane, K. M., Cywin, C. L., Brown, M. L., and Pargellis, C. A. (1997) *Nat. Struct. Biol.* **4,** 311–316
56. Uehata, M., Ishizaki, T., Satoh, H., Ono, T., Kawahara, T., Morishita, T., Tamakawa, H., Yamagami, K., Inui, J., Maekawa, M., and Narumiya, S. (1997) *Nature* **389,** 990–994
57. Mrass, P., Kinjyo, I., Ng, L. G., Reiner, S. L., Puré, E., and Weninger, W. (2008) *Immunity* **29,** 971–985
58. Jensen, P. V., and Larsson, L. I. (2004) *Histochem. Cell Biol.* **121,** 361–369
59. Bourguignon, L. Y., Singleton, P. A., Zhu, H., and Zhou, B. (2002) *J. Biol. Chem.* **277,** 39703–39712
60. Di Guglielmo, G. M., Le Roy, C., Goodfellow, A. F., and Wrana, J. L. (2003) *Nat. Cell Biol.* **5,** 410–421
61. Toole, B. P., Zoltan-Jones, A., Misra, S., and Ghatak, S. (2005) *Cells Tissues Organs* **179,** 66–72
62. Wyatt, T. A., Ito, H., Veys, T. J., and Spurzem, J. R. (1997) *Am. J. Physiol.* **273,** L1007–L1012
63. Anggiansah, C. L., Scott, D., Poli, A., Coleman, P. J., Badrick, E., Mason, R. M., and Levick, J. R. (2003) *J. Physiol.* **550,** 631–640
64. Acharya, P. S., Majumdar, S., Jacob, M., Hayden, J., Mrass, P., Weninger, W., Assoian, R. K., and Puré, E. (2008) *J. Cell Sci.* **121,** 1393–1402
65. Kan, F. W. (1990) *Anat. Rec.* **228,** 370–382